Check for updates

Kinetic analysis to describe Co-operative redox enhancement effects exhibited by bimetallic Au–Pd systems in aerobic oxidation†

Isaac T. Daniel, [iD] [a] Liang Zhao, [iD] [a] Donald Bethell,[a] Mark Douthwaite,*[a]
Samuel Pattisson,[a] Richard J. Lewis, [iD] [a] Ouardia Akdim,[a] David J. Morgan, [iD] [a]
Steven McIntosh [iD] [b] and Graham J. Hutchings [iD] *[a]

Recent work has demonstrated that for bimetallic Au–Pd systems, the rate of catalytic alcohol and formyl dehydrogenation (DH) is intrinsically linked to the rate of oxygen reduction (ORR) within the same system. Herein, the rate enhancement as a result of the coupling between these two processes is assessed *via* kinetic analysis for the oxidative dehydrogenation of 5-hydroxymethylfurfural. The influence of the Au and Pd molar ratio is explored for a physical mixture of carbon-supported catalysts by changing the mass of each 1 wt% catalyst. Importantly, the activity of the bimetallic system exceeds the sum of the monometallic analogues, at all molar ratios. It is shown that by considering the coupling between two individual reactions (DH and ORR), the kinetic analysis of the system predicts where the maxima in monometallic and bimetallic activity will be observed. The accuracy of the model provides further evidence and understanding of cooperative redox enhancement (CORE) effects observed in bimetallic, heterogeneous catalytic systems.

1. Introduction

The combination of Au and Pd to produce supported bimetallic catalysts has led to significant performance enhancements in a variety of important reactions including the oxidative dehydrogenation (ODH) of alcohols and formyls[1–4] and the direct synthesis of H_2O_2.[5–8] Understanding the origin and scope of these enhancement effects is crucial to ensure bimetallic systems are employed in the most effective way. The heightened catalytic efficiency relative to the analogous monometallic systems is often attributed to synergistic effects between the two metals. These can arise from the changing of several different factors, such as coordination number and surface electronic states, and can result in preferable activity and selectivity.[9–11]

Recently, Huang *et al.*[12] developed an alternative approach to explain rate enhancements observed over bimetallic Au–Pd catalytic systems. The authors utilized both thermo- and electro-catalytic methods to study the rate enhancements that

arise when Au and Pd are combined in supported, heterogeneous catalytic systems, with 5-hydroxymethylfurfural (HMF) used as their primary model substrate. HMF is an ideal model to study such reactions, as it possesses both alcohol and formyl functionalities. Crucially, it was determined that by spatially separating the metallic sites, either by using a physical mixture (PM) of monometallic catalysts or through the synthesis of a Janus-type structure, the enhancement exceeded that exhibited by an analogous Au–Pd alloy catalyst.

Heightened performance was observed for both PM and Janus-type systems for the ODH of a range of alcohols and through linear-sweep voltammetry (LSV) experiments, the separation of sites is shown to be essential in maximising the rate of dehydrogenation (DH). It was demonstrated that Au and Pd nanoparticles are individually catalysing distinct half-cell reactions, namely DH and the oxygen reduction reaction (ORR). The activity enhancement for all the 'non-alloyed' bimetallic systems was attributed to the intrinsic coupling of DH occurring over Au sites and the consumption of produced electrons *via* ORR at Pd sites. Pd is known to be much more effective at ORR than Au, with the inverse true for DH, hence it is consistent that the half-cell reactions should predominately take place in this way.[13,14]

The transfer of electrons generated by DH through a conductive support was found to be a significant part of the system and the rate enhancement is diminished with the use

[a] *Max Planck-Cardiff Centre on the Fundamentals of Heterogeneous Catalysis FUNCAT, Cardiff Catalysis Institute, School of Chemistry, Cardiff University, Main Building, Park Place, Cardiff, CF10 3AT, UK. E-mail: douthwaitejm@cardiff.ac.uk, hutch@cardiff.ac.uk*
[b] *Department of Chemical and Biomolecular Engineering, Lehigh University, Bethlehem, PA, USA*
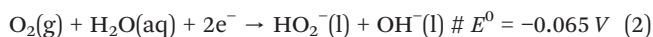
of semi-conducting materials. Overall, this cooperative redox enhancement (CORE) effect observed between Au and Pd is a new observation and differs from the traditionally discussed "synergy" as the individual metallic properties, such as redox potential, are importantly unaltered, as is their individual ability to catalyse each half-cell reaction.

Clearly, this analysis means that the rate of ORR is vital during alcohol and formyl DH and needs to be considered. It was demonstrated that within the CORE system, by increasing the amount of Pd catalyst present, and therefore increasing the rate of ORR, the rate of DH is proportionally (yet indirectly) increased.[12] Using monometallic Au and Pd catalytic systems, Davis et al.[15] extensively investigated the importance of ORR during selective alcohol oxidation. It is demonstrated that at high pH, hydroxide ions are the source of the inserted oxygen atom. This suggests that O_2 plays an important but indirect role within the catalytic cycle; to be the source of hydroxide ions through its reduction prior to dissociation. This work supports our recent discovery,[12] making clear the importance of efficient electron consumption, in this case through oxygen reduction, that leads to CORE effects.

ORR is a comprehensively researched reaction due to its important role in fuel cells.[16–19] The exceptional strength of the O=O double bond (498 kJ mol^{-1}) means the presence of a catalyst is required to avoid excessive energy input.[20] In alkaline media, oxygen reduction can occur via a four electron or two sequential two electron processes (eqn (1)–(3)).[21] Due to the high pH, the initial two electron process will produce an unstable peroxide intermediate of the form HO_2^-, which will undergo rapid reduction to hydroxide ions.[22,23]

$$O_2(g) + 2H_2O(aq) + 4e^- \rightarrow 4OH^-(l) \# E^0 = +0.401\ V \quad (1)$$

$$O_2(g) + H_2O(aq) + 2e^- \rightarrow HO_2^-(l) + OH^-(l) \# E^0 = -0.065\ V \quad (2)$$

$$HO_2^-(l) + H_2O(l) + 2e^- \rightarrow 3OH^-(aq) \# E^0 = +0.87\ V \quad (3)$$

The effectiveness of a catalyst towards ORR is primarily dependant on the strength of binding between oxygen and metal species. As described by The Sabatier Principle,[24] the most active metals bind oxygen to an intermediate degree, allowing reduction but preventing surface poisoning. Pt and Pd are generally known to be the most active metals, lying at the summit of volcano plots that are often used to describe the activity of different metals and surfaces for ORR.[13,14,25] Here, through the matching of kinetic modelling and experimental data, Au and Pd will be seen to reduce oxygen through different pathways at differing rates.

The experimental work presented by Huang et al.[12] focused on the use of HMF as a substrate, hence the important valorisation of HMF will also be the focus of this work. HMF can be obtained from renewable biomass resources through the dehydration of fructose and glucose and is a pivotal platform chemical.[26,27] Through a multistep

process, the full ODH of HMF produces 2,5-furandicarboxylic acid (FDCA), which is an important platform chemical in itself and was named as one of the top 12 value-added chemicals derived from biomass by the U.S. Department of Energy.[28] For example, it has the potential to replace terephthalic acid – the starting monomer in the production of polyethylene terephthalate (PET).[29]

The bimetallic PM catalytic system investigated here will use a constant HMF: total metal (mol : mol) ratio; the Au : Pd molar ratio will be varied by varying the mass of each catalyst used, whilst keeping the total metal moles constant. Previously, CORE effects have only been reported using a fixed molar ratio (4 : 1 (Au : Pd)),[12] hence it is essential to explore where the maxima in rate enhancement is for the combination of these specific catalysts. The sum of the analogous monometallic systems will be used as an activity baseline, with CORE effects responsible for any activity above this. The monometallic systems will be firstly assessed as to whether catalytic activity has a linear (or otherwise) dependency on metal moles. Given that ORR must be occurring even in monometallic situations, the dependency will elucidate if any CORE enhancement is present here due to the single metal performing two catalytic roles (i.e., DH and ORR).

To build a deeper understanding of CORE effects in Au and Pd catalysis,[12] it is important to consider the kinetics of the system. The full DH of HMF can proceed via two routes (Scheme 1) with either the alcohol or formyl oxidation occurring first. We have observed that the alcohol oxidation occurs first almost exclusively when using Au and Pd catalysts,[12] therefore the initial oxidation of HMF to HMFCA will herein be used as the basis from which to build a kinetic understanding. Assumptions made during the kinetic analysis presented are formulated from current understanding of CORE effects in a Au and Pd system. A kinetic model that accurately correlates with the experimental data will further support the proposed system for bimetallic activity enhancement.

2. Experimental

2.1. Chemicals

Chloroauric acid (HAuCl$_4$·3H$_2$O, Strem Chemicals, 99.8%); distilled water (Millipore, 18.2 MΩ cm at 25 °C); 5-hydroxymethylfurfural (Sigma-Aldrich, >99%); palladium chloride (PdCl$_2$, Sigma-Aldrich, >99.9%); polyvinyl alcohol (PVA, Sigma-Aldrich, 80% hydrolysed); sodium borohydride (NaBH$_4$, Sigma-Aldrich, 99.99%); sodium hydrogen carbonate (Fisher Scientific, >99.5%); Vulcan XC72R (Cabot).

2.2. Catalyst preparation – sol immobilisation

The following method was used to synthesise 0.5 g of 1 wt% Au/C and 1 wt% Pd/C catalysts. Aqueous precursor solution (HAuCl$_4$, 11 mg$_{Au}$ mL^{-1} or PdCl$_2$, 5.5 mg$_{Pd}$ mL^{-1}) and PVA (10 mg mL^{-1}, PVA mass : metal mass = 1 : 1) were added to vigorously stirred DI water (140 mL) in a 600 mL glass beaker. After 15 minutes of mixing, freshly prepared NaBH$_4$ (0.15 M, mol : metal mol = 4 : 1) was rapidly added and the resulting sol
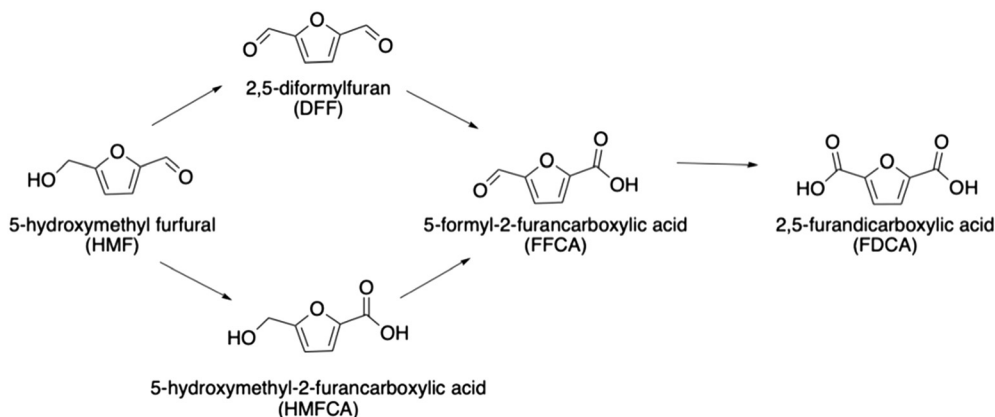
Scheme 1 The oxidative dehydrogenation of HMF can proceed *via* the oxidation of either the alcohol or formyl group first.

stirred for a further 30 minutes. The support material (Carbon Black, Vulcan XC72R, 0.495 g) was added to the colloidal solution and stirred for a further 30 minutes enabling immobilisation. The resulting catalyst was filtered, washed (DI water, 1 L g^{-1}) to remove inorganic ions and dried under static air (110 °C, 16 h).

2.3. HMF oxidative dehydrogenation

A glass Colaver reactor (50 mL) was charged with an aqueous solution (16 mL) of HMF (0.1 M) and NaHCO$_3$ (0.4 M). Under constant stirring (1000 rpm), the solution was allowed to stabilise (10 minutes) at 80 °C before the addition of the catalyst in the requisite amounts. The Colaver was purged 5 times with O$_2$ before pressure was maintained at 3 bar with O$_2$ constantly fed into the system. The molar ratio of Au : Pd was varied by varying the mass of the 1 wt% catalysts used. In bimetallic reactions, the HMF : metal molar ratio was kept constant (200 : 1). Typical reaction time was either 30 or 120 minutes, with samples taken at regular intervals.

Sample analysis was carried out using high-performance liquid chromatography (Agilent Technologies 1200 series) equipped with a diode array detector and a Hi-Plex H (300 × 7.7 mm) column. The mobile phase consisted of 5.5 mM H$_2$SO$_4$ solution at a flow rate of 0.7 mL min^{-1}. Molar quantification, HMF conversion and product selectivity was obtained by pre-determined response factors based on calibrations with known concentrations of HMFCA, FFCA and FDCA. Turnover activity is calculated from molar quantities of the intermediates and products using the equation below.

$$\text{Activity } (\text{mol s}^{-1})$$
$$= \frac{(\text{HMFCA}_{\text{mol}} \times 1) + (\text{FFCA}_{\text{mol}} \times 2) + (\text{FDCA}_{\text{mol}} \times 3)}{\text{Time}(s)} \quad (4)$$

2.4. Catalyst analysis

Inductively coupled plasma atomic emission spectroscopy (ICP-AES) was used to determine metal loading. Catalyst samples were initially digested by microwave radiation before analysis. An Agilent 7900 ICP-MS with I-AS autosampler was used to analyse the digested catalysts for specific metal content. All samples were diluted by a factor of 10 and made up with 500 μL of sample into class A volumetric flasks with DI-H$_2$O (which included 1% HNO$_3$ and 0.5% HCl matrix). For interference reduction, Nickel Sampling and Skimmer cones were used with He mode on the ORS4 Octopol. Certified Reference material from Perkin Elmer (1000/100/10/10/blank μg L^{-1}) was used for five-point calibration, with an Agilent certified internal standard.

Transmission Electron Microscopy (TEM) was conducted on a JEOL 2100-JEM operating at 200 kV. Catalyst samples were analysed as a solid dispersed on holey carbon films on 300 mesh copper grids. At least 100 particles were measured for each catalyst to produce a particle size distribution.

X-ray photoelectron spectroscopy (XPS) was performed on a Thermo Fisher Scientific K-alpha$^+$ spectrometer. Samples were analysed using a micro-focused monochromatic Al X-ray source (72 W) using the "400-micron spot" mode, which provides an analysis defining elliptical X-ray spot of *ca.* 400 × 600 microns. Data was recorded at pass energies of 150 eV for survey scans and 40 eV for high resolution scan with 1 eV and 0.1 eV step sizes respectively. Charge neutralisation of the sample was achieved using a combination of both low energy electrons and argon ions.

Data analysis was performed in CasaXPS v2.3.25 (ref. 30) after calibrating the data to the C(1s) peak maximum at 284.5 eV which is characteristic of the sp2 component of the activated carbon. Quantification was made using a Shirley type background and Scofield cross sections, with an electron energy dependence corresponding to the TPP-2 M method.[31]

3. Results and discussion

3.1. Kinetic model development

Within the proposed bimetallic CORE system, the initial DH of HMF occurs over Au sites, with ORR subsequently occurring over Pd sites. Electrons that are produced during the DH reaction are consumed in the latter ORR reaction. The overall
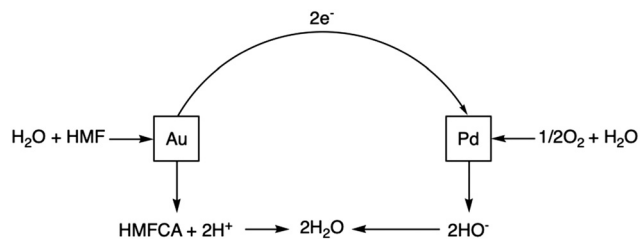
Scheme 2 The proposed CORE system detailing oxidative dehydrogenation occurring over Au sites and oxygen reduction occurring over Pd sites. In the thermocatalytic system, the transfer of electrons occurs through the carbon support.

process can be simply described by Scheme 2 and the accompanying equations (eqn (5) and (6)), with the associated rate constants detailed in Table 1.

In electrochemical experiments, the electron transfer occurs through an external circuit. Under thermocatalytic conditions however, electron transfer is considered to be mediated by the carbon support. This electron transport between metallic sites will be facile and far more rapid that any chemical reaction taking place. Therefore, we will assume that there is no barrier between the Au and Pd activated states. The measurement of electron transfer barriers would subsequently not improve the model's ability to predict experimental behaviour.

$$HMF + H_2O \rightleftharpoons HMFCA + 2H^+ + 2e^- \quad (5)$$

$$\frac{1}{2}O_2 + 2e^- + H_2O \rightarrow 2OH^- \quad (6)$$
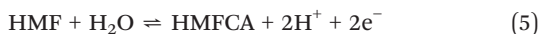
In reactions over heterogeneous catalysts, the substrate (S), is adsorbed to the surface of the metal (M) and it is at this interface (SM) that the reaction takes place. Throughout the subsequent model, the mole fraction of Au will be represented by f. Thus, in bimetallic systems, the mole fraction of Pd will be equal to $(1 - f)$. We can define the total amount of substrate present at any given time (S_T) (eqn (7)) as well as the binding constant, K_a (eqn (8)), for the adsorbed species, under the assumption that $[S]_T \ll [M]$.

$$[S]_T = [S] + [SM] = [SM]\left\{1 + \frac{[S]}{[SM]}\right\} \quad (7)$$

$$K_a = \frac{[SM]}{[S]_T \cdot \{[M] - [SM]\}} \quad (8)$$

When the DH half-cell reaction (eqn (5)) and the binding constant (eqn (8)) are considered, the rate of HMFCA

production (v_1) over a monometallic Au catalyst can be derived (eqn (9)). This is simply a result of the fact that v_1 is proportional to the amount of bound substrate, [SM], which can be substituted from eqn (8). When $K_a [S]_T \gg 1$, i.e., the substrate is in large excess, the rate of HMFCA production is just dependant on the specific rate constant and the amount of Au present. An analogous equation could be derived for Pd.

$$v_1^A = \frac{k_1^A K_a [S]_T [Au]}{1 + K_a [S]_T} \quad (9)$$

In a bimetallic system (eqn (10)), a term is included for substrate interaction at each metallic site and K_a is taken to be an average of the values for Au and Pd.

$$v_1 = \frac{k_1^A K_a [S]_T f \cdot [Au]}{1 + K_a [S]_T} + \frac{k_1^P K_a [S]_T (1 - f) \cdot [Pd]}{1 + K_a [S]_T} \quad (10)$$

In situations where $K_a [S]_T \gg 1$, the equation is simplified (eqn (11)) and (at a constant amount of metal moles) is just dependent on the individual rate constants and the molar ratio of metals.

$$v_1 = [M] \cdot \{k_1^A \cdot f + k_1^P \cdot (1 - f)\} \quad (11)$$

In the proposed CORE system, however, this half-cell reaction is coupled to an ORR (Scheme 2), which itself has an intrinsic effect on the overall rate. Hence, ORR (eqn (1)–(3)) needs to be included into the kinetic analysis. Thus, if eqn (5) and (6) are considered collectively, then basic steady state approximation yields the fact that the rate of HMFCA production at constant metal moles is dependent on a simple expression of rate constants that describe both ODH and ORR (eqn (12)).

$$\frac{v_1}{[M]} \propto \frac{k_1 \cdot k_2}{k_{-1} + k_2} \quad (12)$$

In a monometallic system, the rate constants evidently refer to the active sites on the individual metal present. Within a bimetallic system, at constant total metal moles, the molar ratio as well as which site is catalysing which half-cell reaction will also affect the overall rate. Further to this, in both a monometallic and bimetallic system, oxygen can be reduced by two different pathways (eqn (1)–(3)). For example, it is possible based on the structure of this model that in the bimetallic system, DH and the initial $2e^-$ ORR could occur over Au sites. Subsequently, rapid peroxide reduction, as previously discussed, could occur over Pd sites giving a rate equation of the form of eqn (13). As can be seen, this gives a rate that will be dependent on $f^2(1 - f)$, which would produce

Table 1 Description of rate constants associated with the initial oxidation of HMF to HMFCA as well as the subsequent oxygen reduction reaction

Rate constant	Equation	Descriptor
$k_1^A / k_1^P / k_{-1}$	5	Reversible formation of activated intermediate state over Au (^{A}) or Pd (^{P}) sites
k_2^A / k_2^P	6	Oxygen reduction occurring over Au or Pd sites

a curve with a maximum at 67 mol%. This highlights how differing routes for ORR will result in different shaped bimetallic activity curves.

Overall, with the individual values of k_1 and k_2 assumed to remain constant, it is still the changing of the molar ratio between Au and Pd (*i.e.*, the value of f) along with the oxygen reduction pathway that will affect the rate of HMFCA production. This presents several possible scenarios that can be compared to the experimental data to reveal further insights into the CORE system. Given what we know about the system already,[12] here we will most prominently consider the following: for monometallic Au, DH coupled with $2e^-$ ORR (eqn (14)); and for the bimetallic system, DH occurring on Au coupled with $4e^-$ ORR occurring on Pd (eqn (15)). In the case of the latter, it is important to note that these roles could be reversed, but this is not under consideration here.

$$\frac{\nu_1}{[M]} = \frac{k_1^A f \cdot k_2^A f \cdot k_2^P (1-f)}{k_{-1}} \quad (13)$$

$$\frac{\nu_1}{[M]} = \frac{k_1^A f \cdot k_2^A f}{k_{-1}} \quad (14)$$

$$\frac{\nu_1}{[M]} = \frac{k_1^A f \cdot k_2^P (1-f)}{k_{-1}} \quad (15)$$

With thermocatalytic experiments alone, determination of all the individual rate constants is not possible within the constraints of this model. In the experimental work that follows, a set of HMF oxidation reactions were initially run using varying amounts either 1 wt% Au/C or 1 wt% Pd/C in monometallic systems. 1 wt% catalysts were also used together in a PM in various masses, but with a constant total metal content, to evaluate the activity for HMF conversion. The kinetic model discussed above predicts that certain activity maxima will be seen in certain situations, and this will be compared to the experimental data. Given that the model was formulated based on the current understanding of CORE effects, successfully correlating the activity of the bimetallic system at different molar ratios of Au and Pd would also provide more evidence in support of the CORE system.

3.2. Catalyst characterisation

To begin our experimental investigation, two carbon supported Au and Pd catalysts were prepared *via* sol-immobilisation to a target loading of 1 wt%. Microwave digestion of the solid catalysts followed by ICP-AES analysis confirmed both Au/C and Pd/C had an accurate loading of 1.0 wt% (Table S1†). The carbon support used – Vulcan XC72R – is important due to its high conductivity,[32] which is necessary to facilitate electron transport.

Within our previous work on CORE effects,[12] the Au and Pd catalysts used had a metal loading of 1.75 wt% and 0.25 wt%, respectively. As they were used in a 4:1 molar ratio, the catalysts were synthesised with differing metal loadings to ensure a relatively consistent amount of carbon was used for

each catalyst (in a typical experiment, 72 mg and 71 mg of Au/C and Pd/C were used, respectively). However, subsequent experiments have shown that the addition of blank carbon support to a catalytic system (either monometallic or bimetallic) has no effect on the activity or enhancement (Fig. S1†). Therefore, throughout the experimental work, a consistent loading of 1 wt% is used for both Au/C and Pd/C catalysts. This is to ensure that physical characteristics, such as metal dispersion, are consistent allowing for us to better probe the influence of the Au:Pd ratio.

After synthesis of these materials, they were probed by transition electron microscopy (TEM) to determine the supported metal particle sizes. For this, analysis was conducted on multiple areas of each catalyst. The TEM experiments confirmed that the sol-immobilisation method had been effective, as each catalyst exhibited narrow particle size distributions. Mean particle diameters of 3.0 nm and 4.2 nm were determined for the Au/C and Pd/C catalysts, respectively (Fig. 1). Achieving a small particle size within a tight range is vital to ensure the high activity of supported Au and Pd catalysts, as particle size effects can influence catalytic performance of both DH and ORR.[33–35]

XPS analysis of the Au4f region and Pd3d region was conducted over the respective catalysts (Fig. S2†), which confirms the metallic nature of the Au present. For the fresh Pd/C catalyst, a small proportion of Pd^{2+} is observed with a Pd^0/Pd^{2+} at% ratio of 6.33. The Pd^{2+} species are likely to arise through passivation, which is unsurprising given the reduced Pd/C catalyst is dried at 110 °C in air. Given that electron transfer between Au and Pd is not considered to be limiting, it is not anticipated that the proportion of Pd^{2+} present in the fresh Pd/C catalyst will influence the rate of reaction.

3.3. HMF oxidative dehydrogenation

The Au/C and Pd/C catalysts were subsequently used for the thermocatalytic conversion of HMF. The experimental data (Fig. 2 and 3) discussed here is taken at 30 minutes where initial rates are still valid and the consumption of HMF can be considered a true measure of reaction rate. Initially, both catalysts were reacted separately in monometallic systems and the quantity of each catalyst used was varied to establish how this influenced the activity. Au/C and Pd/C were then used in a physical mixture where the total metal moles was kept constant (HMF: metal = 200:1 (mol:mol)) and the molar ratio between Au and Pd was varied. Throughout these experiments, the molar ratio between Au and Pd was controlled by varying the mass of each 1 wt% catalyst, as opposed to keeping mass constant and altering the weight percent during synthesis. Although this changes the amount of carbon support present, it eliminates any variables that may arise from preparing catalysts with different weight loadings. For this section, results are displayed in terms of activity turnover (eqn (4)) as it accounts for consecutive surface reactions that occur from reaction intermediates. Though, it is important to note that, for both catalysts, the
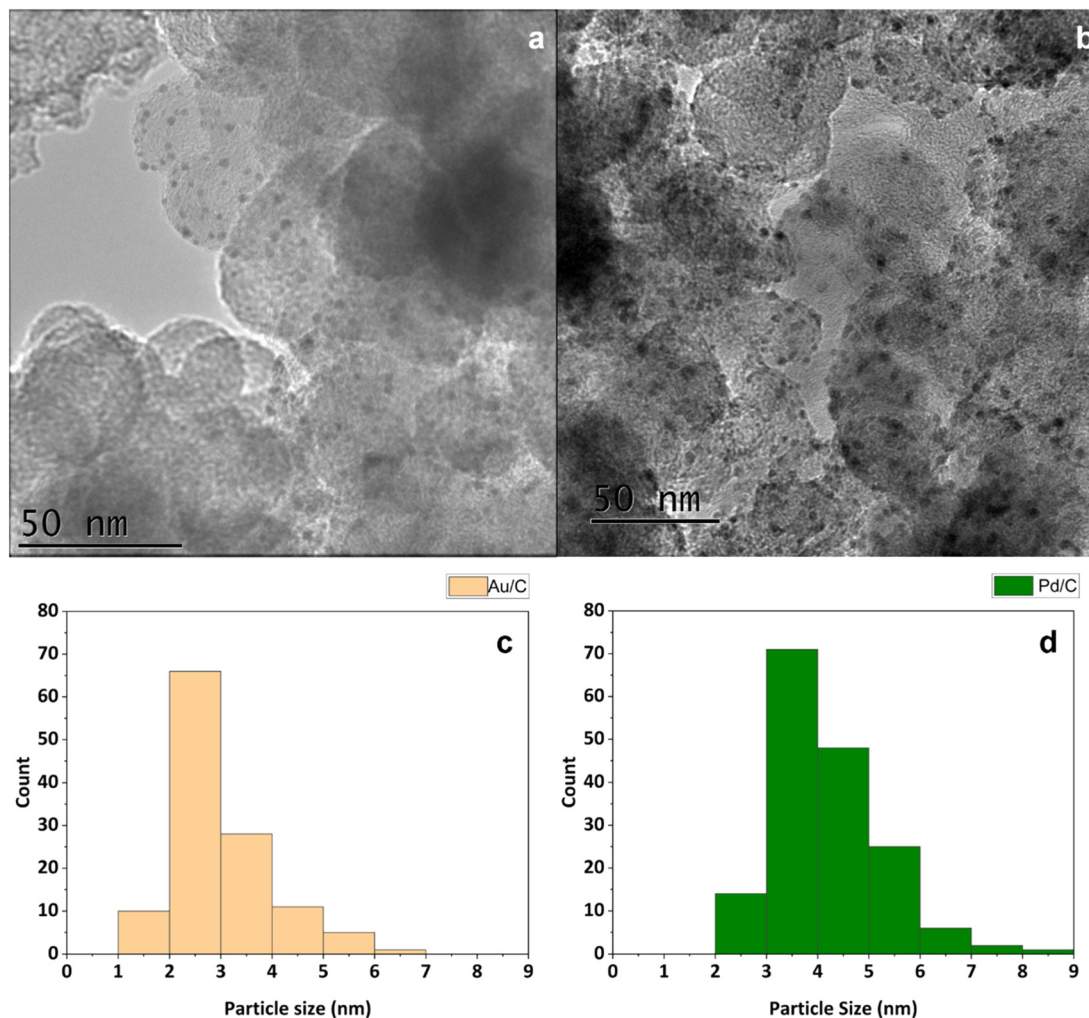
Fig. 1 TEM images and associated particle size distribution of (a and c) 1 wt% Au/C and (b and d) 1 wt% Pd/C. Standard deviation for the particle size of Au/C and Pd/C is 0.9 nm and 1.0 nm, respectively. At least 100 particles were counted in each case.

trends exhibited by these activity measurements are mirrored in the analogous conversion data (Fig. S3†).

Eqn (14) concerns a situation where monometallic Au catalyses both DH and 2e⁻ ORR and gives a scenario where the rate of HMFCA production is proportional to the square of the Au content (f^2). This would give a maximum rate at $f = 1$ and a parabolic relationship between the quantity of Au present and activity. Fig. 2(a) and (c) show how the experimental activity of the Au system correlates with the moles of Au and the square of moles of Au, respectively. Not unexpectedly, the maximum rate is seen at the highest Au content. Somewhat more surprisingly and in line with the kinetic model prediction, there is a clear parabolic relationship. A linear correlation between activity and the square of Au moles is evident at low masses of Au, but this begins to plateau at higher masses. In line with the model, this suggests that CORE is present at low masses in this monometallic system, and that Au does indeed catalyse both DH and ORR, simultaneously. At high moles $(>3.2 \times 10^{-6})$, the relationship tends to be more linear (Fig. 2(a)), indicating

that the kinetic model no longer holds and that one of the half-cell reactions becomes limiting.

Considering the Pd system (Fig. 2(b)), there is a clear linear relationship, demonstrating that the activity is always limited by the rate of the one of the half-cell reactions (likely DH as Pd is a very effective ORR catalyst) and cooperation between the DH and ORR is not enhancing the activity. Fig. 2(d) supports both conclusions for Au and Pd as it can be seen that the productivity of Au increases as the total amount of catalyst increases (until a plateau at high masses). That is to say that the more Au there is present, the more effective each Au site is, which is not the case for Pd. In summary, the Au monometallic system conforms to the kinetic model at low Au masses, showing evidence for coupling between DH and ORR half-cells, which leads to an above-linear enhancement. At high masses of catalyst and throughout the Pd data set, the relationship between activity and metal moles is linear.

Next, the rate of HMF oxidation over physical mixtures of Au/C and Pd/C was investigated. The stability of the Au/C and
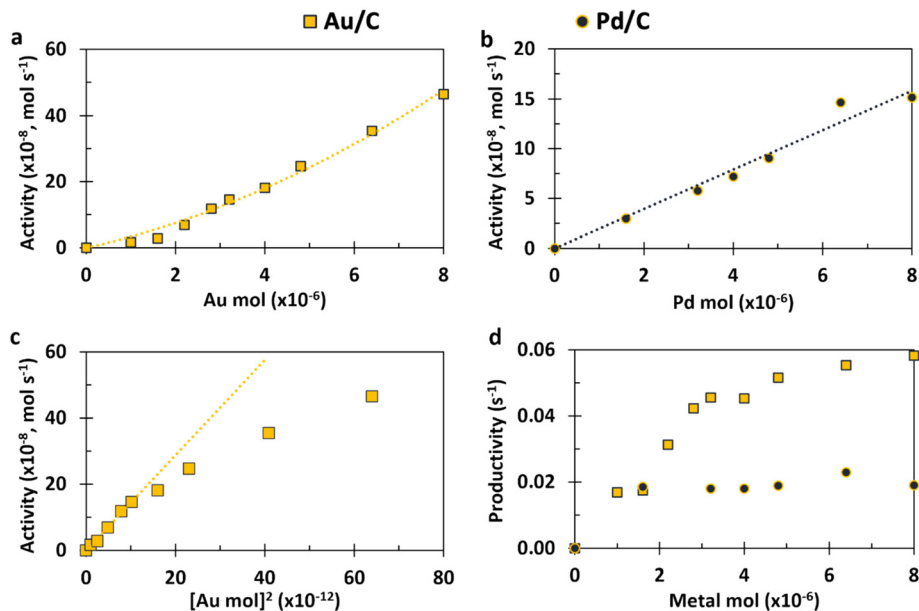
Fig. 2 Experimental data for monometallic systems using varying amounts of either 1 wt% Au/C or 1 wt% Pd/C. (a) Au activity as Au content increases; (b) Pd activity as Pd content increases; (c) Au activity against the square of Au content; (d) productivity (activity per metal moles) of both Au and Pd as metal moles increases. Reaction conditions: H_2O (16 mL), HMF (0.1 M), $NaHCO_3$ (0.4 M), 3 bar O_2, 80 °C, 30 minutes.
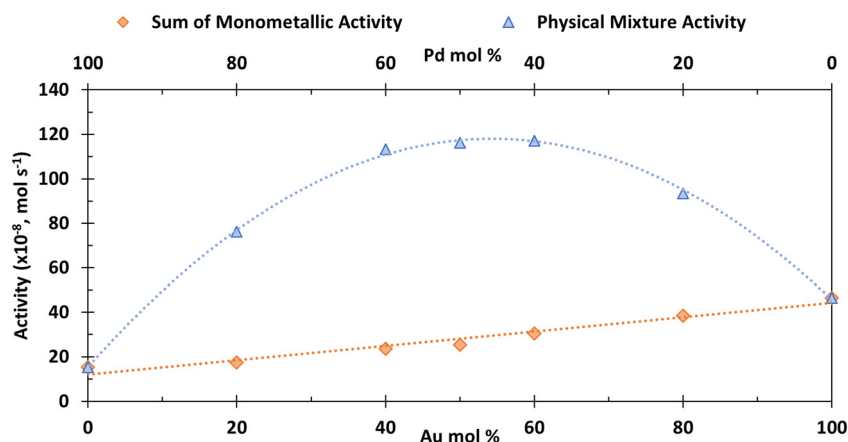

Fig. 3 The sum of monometallic activities compared to physical mixture activities for 1 wt% Au/C and 1 wt% Pd/C at various molar ratios. The total metal content is constant throughout the physical mixture system. The sum of monometallic activities is calculated from the monometallic activity of 1 wt% Au/C and 1 wt% Pd/C at each specific catalyst amount. Error bars represent ± standard deviation for $N = 2$. Reaction conditions: H_2O (16 mL), HMF (0.1 M), $NaHCO_3$ (0.4 M), 3 bar O_2, 80 °C, 30 minutes, HMF mol : metal mol = 200 : 1 for 100 mol%.

Pd/C catalysts, when employed as physical mixtures, is an important consideration that should be addressed.[36,37] Previous studies have demonstrated that Pd can be transferred to Au particles over physical mixtures of supported monometallic Au and Pd catalysts in an organic medium, thus influencing their activity over time. However, the catalyst synthesis and testing conditions used herein align with those used in our previous work,[12] where a variety of techniques were used to assess this. Collectively these experiments demonstrated that no Au or Pd migration occurred, suggesting that under basic aqueous conditions the Au/C and Pd/C catalysts are stable.

Fig. 3 shows that at all molar ratios there is a significant and symmetrical enhancement in activity compared to the sum of the analogous monometallic systems (similar enhancement is seen for HMF conversion (Fig. S4†)). For example, the activity for HMF conversion (× 10^{-8}) of a monometallic Au catalyst at 4 × 10^{-6} mol (50 mol.%) is 18.1 mol s^{-1}; the analogous activity for the same amount of Pd moles in a monometallic system is 7.2 mol s^{-1}. In a physical mixture, when combining these two quantities of catalyst, the activity is 116 mol s^{-1}, which is far in excess of the sum of the two monometallic systems (25.3 mol s^{-1}), hence demonstrating the significant enhancement which is governed by the CORE effect.[12]

The kinetic model formulated based on the CORE effect predicts that the rate of HMFCA production (or the activity as presented here) of the physical mixture will be proportional to $f(1 - f)$ (eqn (15)), which is based the scenario that Au catalysed DH is coupled with Pd catalysed $4e^-$ oxygen reduction. A typical graph of the form $y = f(1 - f)$ is a symmetrical curve with a maxima at $f = 0.5$. From Fig. 3 we can see that the experimental data correlates exceptionally well with this, showing symmetrical enhancements across the molar ratios. Although very close, the activity at 50 mol% is not actually the true maxima, but small derivations are to be expected due to competing ORR pathways always being present. Overall, it can be concluded that kinetic analysis presented here accurately describes the physical mixture system in the case of Au and Pd.

From both Fig. 2 and 3, it is clearly shown that the kinetic model presented, specifically eqn (14) and (15), predict certain experimental activity. The dependence on the molar quantity of Au and/or Pd is varied depending on the catalytic system. However, the coupling between DH and ORR is consistently evident, supporting the assumptions made during the derivation.

4. Conclusion

The kinetic model presented in this work was based upon the novel CORE effect observed in alcohol oxidation reactions.[12] It explains the significant activity enhancement seen when using a Au and Pd bimetallic catalytic system by demonstrating coupling between DH and ORR reactions on separate catalytic sites. Herein, a kinetic model is presented that correctly predicts the relative activity (*i.e.*, the trend and the maxima) of a monometallic Au system, as a correlation was observed between activity and squared metal moles. This is to say that rate of HMFCA production if proportional to f^2. In a bimetallic system, containing a physical mixture of Au and Pd catalysts, the shape and maxima of activity values when the molar ratio is varied is equivalent to that modelled by the kinetic analysis, which predicted a shape proportional to $f(1 - f)$. This provides further evidence in support of the CORE system and emphasises how the rate of ORR is vital in the overall rate of DH of alcohols and formyls. Building from this there are other scenarios (*e.g.*, eqn (13)) that could potentially exist for various bimetallic combinations, where maximum enhancement, if any, is seen at a different molar ratio.

Conflicts of interest

There are no conflicts of interest to declare.

Acknowledgements

References

1 S. Han and C. B. Mullins, *Acc. Chem. Res.*, 2021, **54**, 379–387.

2 N. Dimitratos, J. A. Lopez-Sanchez, D. Morgan, A. F. Carley, R. Tiruvalam, C. J. Kiely, D. Bethell and G. J. Hutchings, *Phys. Chem. Chem. Phys.*, 2009, **11**, 5142–5153.

3 A. Villa, M. Schiavoni, S. Campisi, G. M. Veith and L. Prati, *ChemSusChem*, 2013, **6**, 609–612.

4 J. Pritchard, L. Kesavan, M. Piccinini, Q. He, R. Tiruvalam, N. Dimitratos, J. A. Lopez-Sanchez, A. F. Carley, J. K. Edwards, C. J. Kiely and G. J. Hutchings, *Langmuir*, 2010, **26**, 16568–16577.

5 N. Agarwal, L. Thomas, A. Nasrallah, M. A. Sainna, S. J. Freakley, J. K. Edwards, C. R. A. Catlow, G. J. Hutchings, S. H. Taylor and D. J. Willock, *Catal. Today*, 2021, **381**, 76–85.

6 J. K. Edwards, B. E. Solsona, P. Landon, A. F. Carley, A. Herzing, C. J. Kiely and G. J. Hutchings, *J. Catal.*, 2005, **236**, 69–79.

7 Y. Yi, L. Wang, G. Li and H. Guo, *Catal. Sci. Technol.*, 2016, **6**, 1593–1610.

8 J. K. Edwards, E. N. Ntainjua, A. F. Carley, A. A. Herzing, C. J. Kiely and G. J. Hutchings, *Angew. Chem., Int. Ed.*, 2009, **48**, 8512–8515.

9 A. Groß, *Top. Catal.*, 2006, **37**(1), 29–39.

10 H. C. Ham, G. S. Hwang, J. Han, S. W. Nam and T. H. Lim, *J. Phys. Chem. C*, 2010, **114**, 14922–14928.

11 A. K. Singh and Q. Xu, *ChemCatChem*, 2013, **5**, 652–676.

12 X. Huang, O. Akdim, M. Douthwaite, K. Wang, L. Zhao, R. J. Lewis, S. Pattisson, I. T. Daniel, P. J. Miedziak, G. Shaw, D. J. Morgan, S. M. Althahban, T. E. Davies, Q. He, F. Wang, J. Fu, D. Bethell, S. McIntosh, C. J. Kiely and G. J. Hutchings, *Nature*, 2022, **603**, 271–275.

13 A. Kulkarni, S. Siahrostami, A. Patel and J. K. Nørskov, *Chem. Rev.*, 2018, **118**, 2302–2312.

14 J. K. Nørskov, J. Rossmeisl, A. A. Logadottir, L. Lindqvist, J. R. Kitchin, T. Bligaard and H. Jónsson, *J. Phys. Chem. B*, 2004, **108**, 17886–17892.

15 B. N. Zope, D. D. Hibbitts, M. Neurock and R. J. Davis, *Science*, 2010, **330**, 74–78.

16 S. Sui, X. Wang, X. Zhou, Y. Su, S. Riffat and C. J. Liu, *J. Mater. Chem. A*, 2017, **5**, 1808–1825.

17 F. D. Sanij, P. Balakrishnan, P. Leung, A. Shah, H. Su and Q. Xu, *Int. J. Hydrogen Energy*, 2021, **46**, 14596–14627.

18 S. Zaman, L. Huang, A. I. Douka, H. Yang, B. You and B. Y. Xia, *Am. Ethnol.*, 2021, **133**, 17976–17996.

19 F. Jaouen, E. Proietti, M. Lefèvre, R. Chenitz, J. P. Dodelet, G. Wu, H. T. Chung, C. M. Johnston and P. Zelenay, *Energy Environ. Sci.*, 2010, **4**, 114–130.

20 R. Ma, G. Lin, Y. Zhou, Q. Liu, T. Zhang, G. Shan, M. Yang and J. Wang, *npj Comput. Mater.*, 2019, **5**(1), 1–15.

21 K. G. C. Senarathna, H. M. S. P. Randiligama and R. M. G. Rajapakse, *RSC Adv.*, 2016, **6**, 112853–112863.

22 Z. Qiang, J. H. Chang and C. P. Huang, *Water Res.*, 2002, **36**, 85–94.

23 X. Zhang, X. Zhao, P. Zhu, Z. Adler, Z.-Y. Wu, Y. Liu and H. Wang, *Nat. Commun.*, 2022, **13**(1), 1–11.

24 P. Sabatier, *Ber. Dtsch. Chem. Ges.*, 1911, **44**, 1984–2001.

25 A. J. Medford, A. Vojvodic, J. S. Hummelshøj, J. Voss, F. Abild-Pedersen, F. Studt, T. Bligaard, A. Nilsson and J. K. Nørskov, *J. Catal.*, 2015, **328**, 36–42.

26 J. N. Chheda, Y. Román-Leshkov and J. A. Dumesic, *Green Chem.*, 2007, **9**, 342–350.

27 S. E. Davis, L. R. Houk, E. C. Tamargo, A. K. Datye and R. J. Davis, *Catal. Today*, 2011, **160**, 55–60.

28 T. Werpy and G. Petersen, *Top Value Added Chemicals from Biomass Volume I-Results of Screening for Potential Candidates from Sugars and Synthesis Gas*, 2004.

29 A. Gandini, A. J. D. Silvestre, C. P. Neto, A. F. Sousa and M. Gomes, *J. Polym. Sci., Part A: Polym. Chem.*, 2009, **47**, 295–298.

30 N. Fairley, V. Fernandez, M. Richard-Plouet, C. Guillot-Deudon, J. Walton, E. Smith, D. Flahaut, M. Greiner, M. Biesinger, S. Tougaard, D. Morgan and J. Baltrusaitis, *Applied Surface Science Advances*, 2021, **5**, 100112.

31 S. Tanuma, C. J. Powell and D. R. Penn, *Surf. Interface Anal.*, 1994, **21**, 165–176.

32 S. Pérez-Rodríguez, E. Pastor and M. J. Lázaro, *Electrochemical behavior of the carbon black Vulcan XC-72R: influence of the surface chemistry*, 2018.

33 N. Dimitratos, J. A. Lopez-Sanchez, D. Lennon, F. Porta, L. Prati and A. Villa, *Catal. Lett.*, 2006, **108**(3), 147–153.

34 C. Megías-Sayago, A. Lolli, D. Bonincontro, A. Penkova, S. Albonetti, F. Cavani, J. A. Odriozola and S. Ivanova, *ChemCatChem*, 2020, **12**, 1177–1183.

35 O. Schade, P. Dolcet, A. Nefedov, X. Huang, E. Saraçi, C. Wöll and J.-D. Grunwaldt, *Catalysts*, 2020, **10**, 342.

36 C. M. Olmos, L. E. Chinchilla, A. Villa, J. J. Delgado, A. B. Hungría, G. Blanco, L. Prati, J. J. Calvino and X. Chen, *J. Catal.*, 2019, **375**, 44–55.

37 D. Wang, A. Villa, P. Spontoni, D. S. Su and L. Prati, *Chem. – Eur. J.*, 2010, **16**, 10007–10013.